EJNMMI Research

ORIGINAL RESEARCH

Open Access

# Diagnostic value and interpretability of [$^{18}$F]FDG-PET/CT radiomics in infective endocarditis

Paola Anna Erba[1,2,3,4,16*], Roberta Zanca[5,6], Martina Sollini[7,8], Lara Cavinato[9], Alessandra Ragni[9], Derk Ten Hove[3], Andor WJM Glaudemans[3], Santiago Aguadè-Bruix[10,11], Maria N. Pizzi[10,11,12], Albert Roque[10,11,13], Francesca Ieva[9,14] and Riemer HJA Slart[3,15]

## Abstract

**Background** to assess the value of [18 F]FDG PET/CT radiomics in infective endocarditis (IE) diagnosis. We evaluated and collected [18 F]FDG PET/CT and clinical data of 447 patients, with suspected IE studied in 3 centers. Radiomic features were calculated and after dimensionality reduction, we performed: (1) univariate testing for assessing the discrimination power of clinical variables and radiomics; (2) a multivariate random forest-based model fed by radiomics to predict the outcome of PET/CT visual analysis; (3) a clustering-based radiomic model to predict final diagnosis; (4) a series of Logistic Regression (LR) models to assess the relative contribution of each criterion in relation with final diagnosis.

**Results** 9/17 clinical and 7/11 radiomics variables were able to univariately stratify patients. The random forest model accurately predicted PET/CT visual assessment in definite cases, providing a classification of doubtful cases resembling the "IE-negative" radiomic signature. The clustering-based analysis divided patients in two groups. LRs demonstrated that the richer the information fed into the model, the higher the performances: the models including radiomics performed better than the one solely including visual image assessment.

**Conclusion** Radiomic signature, employing both supervised and unsupervised approaches, effectively described and differentiated [18 F]FDG PET/CT outcomes in a large IE cohort. The identification of specific signatures for equivocal PET/CT findings suggests that radiomic features can assist in interpreting ambiguous PET results, thus significantly impacting patient management. Clustering algorithm successfully associated patients with varying conditions, allowing for further assessment and characterization within the radiomics framework, potentially leading to risk score-based interpretations.

*Correspondence:
Paola Anna Erba
paolaanna.erba@unimib.it

Full list of author information is available at the end of the article

## Introduction

Infective endocarditis (IE) is still a deadly disease with a high hospital mortality ranging from 15% in Pace Maker/Implantable Cardioverter Defibrillator (PM/ICD) endocarditis, up to 16% in Native Valve Endocarditis (NVE), and up to 20% in Prosthetic Valve Endocarditis (PVE) [1]. Since the 1994, with the introduction of the Duke criteria [2] and later modifications [3–5], the diagnosis of infective endocarditis relies on the presence of a number of major/minor criteria to confirm (i.e., definite) or continue to consider (i.e., possible) the suspicion of the disease. Microbiology carries weight amongst these criteria, but culture-negative IE often hampers the diagnosis. Moreover, culture-negative IE are emerging as a clinical challenge as recently shown by the EURO-ENDO registry [1]. Besides microbiology, echocardiography – the second pillar in the diagnostic flowchart of IE – has also limited value in some circumstances, e.g.in the presence of prosthetic valve(s) and cardiac device(s). For these reasons, the 2015 ESC Guidelines for IE introduced new strategies to improve diagnosis and prognosis and to reduce their level of uncertainty. Molecular imaging was inserted among the novelties of the 2015 ESC criteria [5] and its role was confirmed in the latest 2023 ESC criteria [3]. [$^{18}$F]FDG PET/CT, in association with the Duke criteria, has proven to reduce the number of "possible" PVE, providing a conclusive diagnosis (i.e., definite/reject) [6–12] without significant decrease in specificity [13]. In the case of NVE, [$^{18}$F]FDG PET/CT showed lower sensitivity despite imaging interpretation was considered more straightforward than in PVE. However, such result was offset by a near perfect specificity for detection of NVE and an unrivaled ability to identify septic emboli [14, 15]. Nevertheless, even if all these data confirmed that [$^{18}$F]FDG PET/CT may assist in the diagnosis of IE, it presents some drawbacks including adequate patients' preparation [16], and imaging reading and reporting, as for other domains of infection and inflammation [17]. In this regard, a multidisciplinary approach encompassing a huge expertise in the field and a deep knowledge of potential pitfalls is crucial to properly interpret images. Especially in "possible" cases or in presence of unexperienced imagers, visual analyses might benefit from quantitative radiomic parameters (i.e., quantitative descriptors mathematically extracted from images) which may assist in the diagnostic interpretation. Although the latest years have shown an increasing literature on radiomics [18–20], appropriate methods for study design, image and data analyses are still to be defined, resulting in limited clinical evidence in particular in the field of cardiovascular infections [21]. Indeed, most of the published data are applied to oncology and based on the analysis of (too) many features in small monocentric cohorts, limiting radiomics trustworthiness. Furthermore, radiomics thus far was never explained through pathophysiology and rarely compared to known prognostic/predictive markers, visual analyses and/or a gold standard. Most often it appears to clinicians as an enigmatic black box rather than a well-defined scientific discipline. With this study, we aim to fill this gap, using radiomic analysis in a large multicenter dataset of patients with suspected IE, with the scope of defining the applicability of a radiomic models to increase the diagnostic accuracy in clinical practice.

## Materials and methods

### Population

In this study, we prospectively enrolled a series of 447 patients (284 males and 163 females) with suspected IE between January 2015 and June 2020, in three European nuclear medicine centers (University of Pisa (n = 222), University Medical Center Groningen (n = 83), and Hospital Universitari Vall d'Hebron Barcelona (n = 142)). Data on the type and timing of cardiac surgery, clinical risk factors for IE, microbiology and biochemical blood tests, information on antimicrobial treatment (if applicable), concomitant medications, and echocardiography were collected for all patients. Echocardiography and [$^{18}$F]FDG PET/CT scans with a maximum lag of 7 days. The modified Duke and 2015 IE ESC criteria were employed to classify each patient in one of the three categories: "definite", "possible" and "rejected" IE. The conclusive diagnosis was determined based on the 2015 ESC criteria [5], with a consensus reached by the Endocarditis team at the time of evaluation. Baseline patients' characteristics and IE risk factors are summarized in Table 1. Echocardiography at admission was positive in 227 patients (51%), negative in 130 patients (29%), doubtful in 16 patients (4%), not available in 74 patients (16%). Blood cultures were positive in 323 patients (72%), negative in 124 patients (28%). The most frequent identified pathogens were *S.Aureus* (67 patients, 21%), *E.faecalis* (87 patients, 27%), *Staphylococci spp.* (60 patients, 18%), *Streptococci spp.* (70 patients, 21%) and Other (42 patients, 13%).

### [$^{18}$F]FDG PET/CT preparation, acquisition, and visual image analysis

Prior to PET/CT imaging, all patients underwent preparation involving a 24-hour high-fat and low-carbohydrate (HFLC) diet, followed by 12-hour fasting period. The dietary regimen aimed to effectively suppress the physiological myocardial uptake of [$^{18}$F]FDG [16]. The image acquisition was performed using accredited EARL scanners (for details see Supplemental Table 1), adhering to the EANM Guidelines [16]. Approximately 60 min after intravenous injection of 2.5–5.0.5.0 MBq/kg body weight of [$^{18}$F]FDG, the images were acquired. Detailed parameters for image acquisition and reconstruction are

**Table 1** Main patients features and risk factors including clinical variables in IE-positive and IE-negative groups and associated p-valuesin Table 1 can we correct age using just 2 decimal as for the other values?

| | IE-positive (227) | IE-negative (130) | *p*-value |
|---|---|---|---|
| **Age** | 6860.53 ± 1642.29 | 6679.26 ± 1691.47 | 0.301 |
| **Sex** | | | 0.306 |
| F | 86 (38%) | 43 (33%) | |
| M | 141 (62%) | 87 (67%) | |
| **Atrial fibrillation** | | | 0.553 |
| YES | 57 (25%) | 27 (21%) | |
| NO | 170 (75%) | 103 (79%) | |
| **Steroids** | | | 0.824 |
| YES | 45 (20%) | 39 (17%) | |
| NO | 182 (80%) | 188 (83%) | |
| **Previous IE** | | | 0.592 |
| YES | 50 (22%) | 22 (19%) | |
| NO | 177 (78%) | 105 (81%) | |
| **Previous antimicrobial treatment** | | | 0.734 |
| YES | 104 (46%) | 56 (43%) | |
| NO | 123 (54%) | 74 (57%) | |
| **Echo aneurysm** | | | 0.999 |
| YES | 9 (4%) | 130 (100%) | |
| NO | 218 (96%) | 0 (0%) | |
| **Side of IE** | | | 0.658 |
| Right-sided | 120 (53%) | 69 (53%) | |
| Left-sided | 107 (47%) | 61 (47%) | |
| **Diabetes** | | | 0.013 |
| YES | 66 (29%) | 22 (17%) | |
| NO | 161 (71%) | 108 (83%) | |
| **Embolic manifestation** | | | 0.016 |
| YES | 48 (21%) | 10 (8%) | |
| NO | 179 (79%) | 120 (92%) | |
| **Ongoing antimicrobial treatment** | | | 0.001 |
| YES | 188 (83%) | 88 (68%) | |
| NO | 39 (17%) | 42 (32%) | |
| **Duration of antimicrobial treatment** | 48.04 ± 126.47 | 20.04 ± 51.15 | 0.001 |
| **Type of valve** | | | 0.002 |
| NVE | 36 (16%) | 39 (30%) | |
| PVE | 191 (84%) | 91 (70%) | |
| **Number of devices** | 1.36 ± 0.89 | 0.91 ± 0.72 | < 0.001 |
| **Time from implantation to PET** | 1612.08 ± 1916.40 | 870.31 ± 1123.26 | 0.001 |
| **Time from implantation to IE** | 1361.68 ± 1821.20 | 249.52 ± 423.38 | < 0.001 |
| **Echo abscess** | | | < 0.001 |
| Positive | 27 (12%) | 0 (0%) | |
| Negative | 200 (88%) | 130 (100%) | |
| **Culture type** | | | |
| Enterococcus | 29 | 25 | |
| Staphylococcus | 32 | 32 | |
| Streptococcus | 32 | 21 | |
| Other | 24 | 19 | |
| **Antimicrobial treatment type** | | | |
| Daptomycin | 24 | 5 | |
| Piperacillin | 9 | 4 | |
| Tazobactam | 8 | 4 | |
| Gentamycin | 12 | 2 | |
| Amoxicillin | 20 | 3 | |

**Table 1** (continued)

| | IE-positive (227) | IE-negative (130) | *p*-value |
|---|---|---|---|
| Clavulanic acid | 16 | 3 | |
| Ceftriaxone | 12 | 5 | |
| Ampicillin | 3 | 7 | |
| **Vegetation** | | | |
| Aortic | 86 | 0 | |
| Mitral | 41 | 1 | |
| Tricuspid | 8 | 0 | |
| Pulmonary | 224 | 131 | |
| **Site of valve** | | | |
| Aortic | 174 | 108 | |
| Mitral | 68 | 28 | |
| Tricuspid | 17 | 11 | |
| Ascending aorta | 13 | 10 | |
| Pulmonary | 8 | 6 | |

Summary statistics are provided in terms of z-standardized mean values standard deviation for continuous variables and percentages for categorical variables

provided in Supplemental Tables 1 and 2. Visual analyses included the evaluation of both attenuation-corrected (AC) and nonattenuation corrected (NAC) images. The interpretation of the images was carried out by PET/CT cardiovascular imagers highly experienced in IE. Firstly, the PET/CT images were visually examined by expert readers (PAE, MNP, AR, RS) to determine the presence of increased [$^{18}$F]FDG uptake at the valvular plane/perivalvular region in comparison to the background (cardiac positive vs. negative). Subsequently, in cases where cardiac [$^{18}$F]FDG uptake was observed, the pattern was characterized as either diffuse-heterogeneous, focal, multifocal, or linear, as suggested by previous works and procedural recommendations [16, 22]. Lastly, any other sites displaying increased [$^{18}$F]FDG uptake were anatomically localized, described, and assessed for the presence of (distant) septic emboli or portal of entry (extra-cardiac positive vs. negative).

### Radiomic features extraction

The quantitative analysis of the PET data was performed by two experts (RZ and PAE), using a commercial software (PET VCAR, GE Healthcare, Waukesha, WI, USA) to semi-automatically delineate a volume of interest (VOI) for the cardiac lesions, using a 40%-$SUV_{max}$ threshold. Manual adjustments were made to the VOI as necessary. LIFEx software (www.lifex.org [23], version 4.9) was employed to extract 44 radiomic features listed in Supplemental Table 2. Details about features calculation report according to the Imaging Biomarkers Standardization Initiative (IBSI) [24] are reported in Supplemental Table 2.

### Statistical and data analyses

Descriptive statistics were employed to evaluate the study population in terms of demographic and clinical variables. This analysis involved the assessment of contingency tables and proportion tests.

#### *Exploratory univariate analysis*

We conducted an in-depth exploration of the radiomics variables. A correlation matrix was constructed to identify features with a correlation exceeding 0.75. The exclusion of features was performed randomly, resulting in 21 features being retained. Subsequently, we employed Principal Component Analysis (PCA) to achieve dimensionality reduction. We set the threshold at 95% explained variability, resulting in the retention of the first 11 principal components. Based on the final diagnosis of IE (IE = 1 vs. IE = 0, with cases of doubtful IE excluded from the analysis), the patients were stratified into two groups. Manova tests were then conducted to assess potential differences in the distribution of the radiomic variables between the groups.

#### *Predictive power of radiomics*

To assess the predictive value of radiomics in distinguishing between different outcomes of [$^{18}$F]FDG PET/CT (i.e., cardiac positive vs. negative), a classification model was developed. Following the preprocessing of features, including correlation-based feature selection and PCA as described above, we employed the Synthetic Minority Over-sampling Technique (SMOTE) to augment the data and adjust for class imbalance. SMOTE generated new samples for the minority class using a K-nearest neighbors (KNN) algorithm, resulting in equal frequencies for the absent IE, present IE, and doubt IE groups (147 samples each). A Random Forest model was then implemented, utilizing Out-of-Bag (OOB) error evaluation. This evaluation was performed exclusively on patients with a definitive diagnosis of either "absent" or "present" IE, to ensure a more robust analysis. Subsequently, the

model was applied to the "doubt" patients to investigate their likelihood to the two definite groups.

#### *Association between radiomics and other variables*

A clustering-based patient stratification approach was employed to establish and understand the associations between radiomics features and clinical variables, as well as the Duke criteria. To this aim, the data was prepared using the same data wrangling methodology (correlation-based feature selection followed by a PCA). Subsequently, we applied Affinity Propagation (AP) clustering [25] with a specified number of clusters (k = 2). The resulting clusters were then interpreted in relation to relevant clinical variables, such as the type of valves, number of devices, Duke criteria, diagnosis of IE, and PET outcome.

#### *Comparison between clinical variables, Duke criteria and radiomics*

The diagnostic utility of [$^{18}$F]FDG PET/CT (i.e., cardiac positive vs. negative) and radiomics in comparison to the traditional Duke criteria, considering the trade-off between cost and benefit, was assessed conducting a series of comparisons involving different models with increasing levels of information and complexity. Specifically, we developed seven Logistic Regression models to predict the final diagnosis of IE, each incorporating a distinct combination of clinical, Duke criteria, and radiomic variables (see Supplemental Table 3). All models underwent cross-validation, with 75% of the dataset utilized as the training dataset and the remaining 25% serving as the test dataset at each iteration. Clinical features were included in the models only when their percentage of missing values was below 30% and they demonstrated statistical significance in univariate testing (using chi-squared test for categorical variables and univariate logistic regression for numerical variables). Each model was compared in terms of its sensitivity, specificity, and accuracy, providing a comprehensive evaluation of its performance. For all analyses, a $p < 0.05$ was considered statistically significant.

All the analysis were carried out through the software R.

## Results

Our cohort consisted of 93 NVE and 354 PVE. Patients were classified according to the modified Duke criteria in 103 definite, 204 possible, and 140 rejected IE. According to the 2015 ESC criteria, 207, 132, and 108 patients were defined as definite, possible, and rejected IE, respectively. Because IE is diagnosed using probability-based criteria (e.g., Duke/ESC), the category "possible IE" carries inherent diagnostic uncertainty. Nevertheless, given the high mortality of the disease, these patients are typically managed with IE-directed antimicrobial therapy even without definitive confirmation. Accordingly, we evaluated diagnostic performance in a high-risk high probability of disease cohort, defined a priori as patients with either "definite IE" or "possible IE." Final diagnosis established and excluded the diagnosis of IE in 293 and 154 cases, respectively.

Overall, for "definite IE" the modified Duke Criteria were more specific than sensitive (94.74% 95% CI:73.97–99.87% versus 89.29% (95% CI:80.63–94.98%), with a positive predictive value of 98.68% (95% CI:91.75–99.80%). If we considered both the category of "definite IE" and "possible IE" we observed a slight improvement of performance (sensitivity = 92.45%, 95% CI:88.03–95.62%, specificity = 96.84%, 95% CI:91.05–99.34%, positive predictive value = 98.49%, 95% CI:95.54–99.50%, negative predictive value 85.19%, 95% CI:78.19–90.22%). Accuracy was 90.29% (95% CI:82.87–95.25%) and 93.81% (95% CI:90.50–96.23.50.23%) for the modified Duke Criteria "definite IE" and "definite IE" plus "possible IE" categories, respectively. Using the ESC Criteria 2015, the "definite IE" category presented a sensitivity of 99.51% (95% CI:97.29–99.99%) with a specificity of 92.86% (95% CI:66.13–99.82%), a positive predictive value of 98.54% (95% CI:97.45–99.16%), and a negative predictive value of 92.86% (95% CI:64.67–98.93%). The use of the 2015 ESC Criteria for both "definite IE" and "possible IE" categories resulted in a sensitivity of 95.31% (95% CI:92.11–97.48%), a specificity of 99.83% (95% CI:99.07–100%), a positive predictive value of 98.88% (95% CI:96.69–99.62%), and a negative predictive value of 97.85% (95% CI:96.41–98.73%). Accuracy was 98.08% (95% CI:96.17–99.89%) and 98.39% (95% CI:97.32–99.12%) for the 2015 ESC Criteria "definite IE" and "definite IE" plus "possible IE" categories, respectively. The difference in diagnostic performances of echocardiography and [$^{18}$F]FDG PET/CT in the different subgroup of patients with NVE, and PVE on biological and mechanical valve subtype are shown in Supplemental Table 4.

### Exploratory results

Table 1 provides a comprehensive overview of the main differences observed within the study population for what regards clinical and demographic information of patients. Concerning the exploratory statistical assessment of the univariate discrimination power of radiomics features,, 7/11 principal components resulted significant at testing ($p < 0.1$), suggesting an association between radiomics and final diagnosis (Supplemental Table 5).

### [$^{18}$F]FDG PET/CT visual analyses

Visually, cardiac uptake at [$^{18}$F]FDG PET/CT (major criterion) was observed in a total of 420, among which 234 were patients with definite IE (25 NVE and 209 PVE, 141 biological and 68 mechanical), 123 patients with possible

IE (19 NVE and 104 PVE, 65 biological and 39 mechanical), and 63 patients with rejected IE (12 NVE and 51 PVE, 31 biological and 20 mechanical). Typical [$^{18}$F]FDG PET/CT uptake pattern (as defined by the 2023 ESC criteria [3]), was found in 370 patients.

An additional 50 patients were classified as positive despite not simultaneously displaying all typical features. These were categorized as positive with an atypical pattern (e.g., heterogeneous and focal uptake of mild intensity, or a heterogeneous diffuse pattern rather than the classic heterogeneous focal pattern). Patients with equivocal findings—corresponding to a homogeneous, linear FDG uptake pattern on PET/CT—numbered 34. Extracardiac foci of [$^{18}$F]FDG uptake were found in 170 cases (38%), interpreted as embolism in 147 patients (33%) (as reported on Table 1) and as portal of entry in 23 patients (5%) (Figs. 1, 2, 3 and 4).

Of interest, the presence of a major [$^{18}$F]FDG PET/CT criterion was observed in 39% of patients without major echo criteria.

### [$^{18}$F]FDG PET/CT cardiac prediction results

The univariate analysis assessed a considerable discriminative power of radiomics in relation to the final diagnosis. Besides, with the radiomics-based random forest, we aimed to assess the multivariate prediction power of radiomics in relation to the visual analysis. The model effectively differentiated between patients with positive and negative [$^{18}$F]FDG PET/CT findings at visual analysis. The performance of the radiomics model, as assessed through the OOB estimate of error rate, yielded a performance of 7.07% (10.87% in the negative class and 3.26% in the positive class). Of interest, when tested on the 34 patients who presented an equivocal [$^{18}$F]FDG uptake pattern, the random forest model classified four patients as "cardiac positive" and 30 as "cardiac negative." The features contributing to this classification included both shape descriptors (e.g., volume, sphericity, compacity) and texture features derived from GLCM, GLRLM, GLZLM, and NGLDM matrices. Notably, among the patients classified as "cardiac negative," the model identified radiomic profiles that closely resembled those of

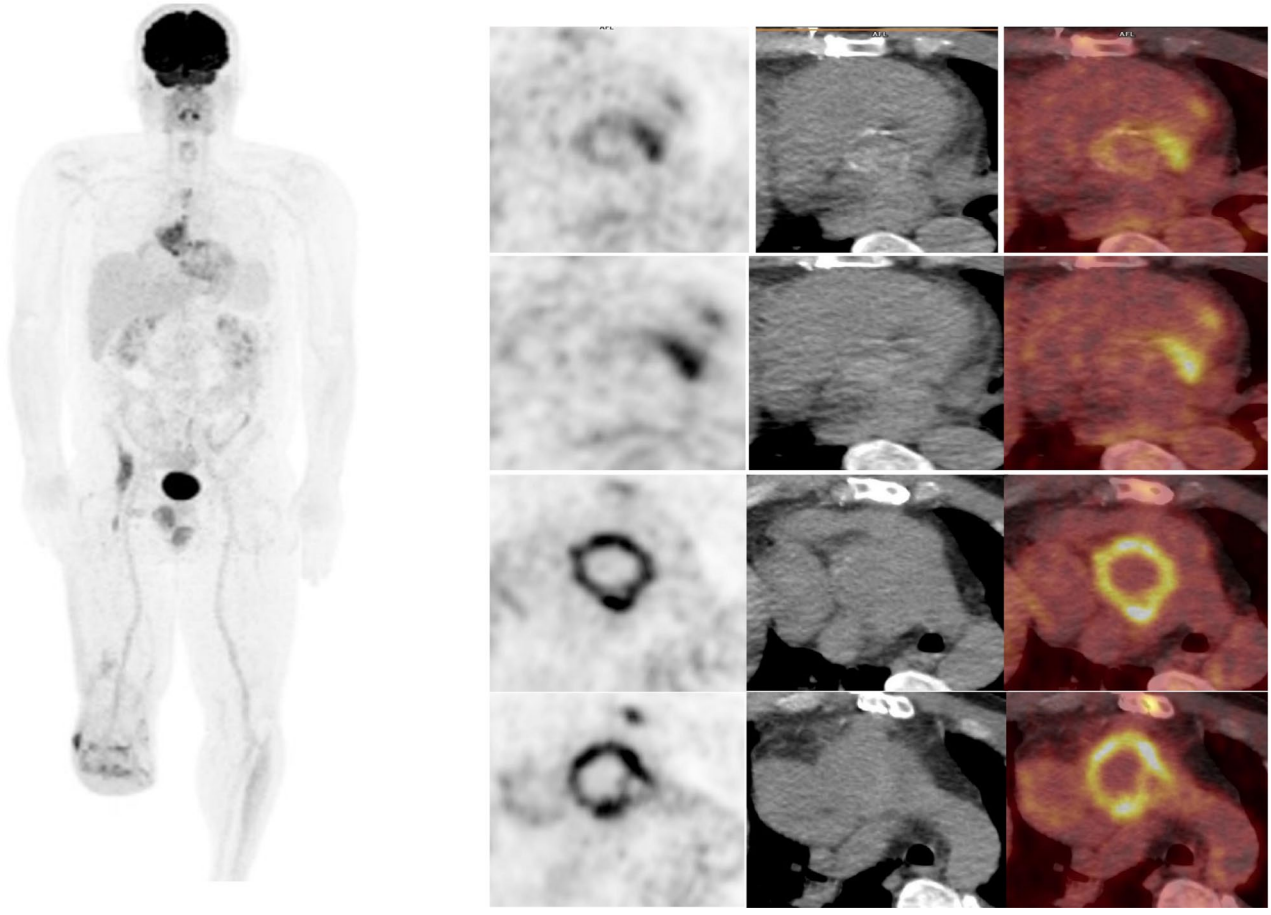

**Fig. 1** [$^{18}$F]FDG PET/CT scan in a patient with IE from Methicillin-Sensitive Staphylococcus aureus (*MSSA)* on a composite aortic valve and ascending aorta mechanical prosthesis. Sequential transaxial emission, CT, and superimposed PET/CT (left to right) images reconstructed for valve plane and Maximum intensity projection (MIP) whole body image (left) shows a diffuse heterogeneous uptake at the level of the PVE extending all around the valve anulus

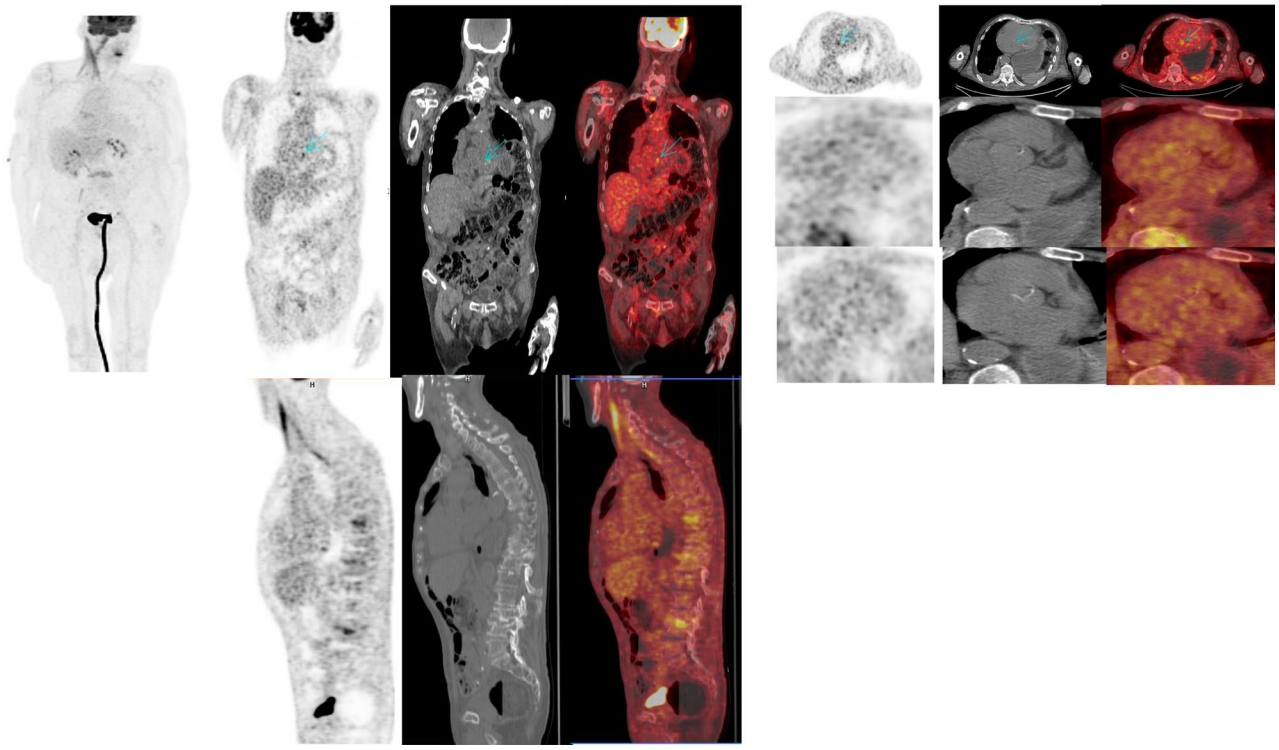

**Fig. 2** [$^{18}$F]FDG PET/CT scan in a patient with IE from *St. lugdunensis* on native valve. Coronal and sagittal whole-body images (middle panel, from left to right transaxial emission, CT and superimposed PET/CT), MIP (left panel) and transaxial images (from left to right emission, CT and superimposed PET/CT) of the thorax (right upper) and reconstructed for valve planes (right middle and lower) show a focal uptake of mild intensity and small size at the site of the native valve confirming the diagnosis

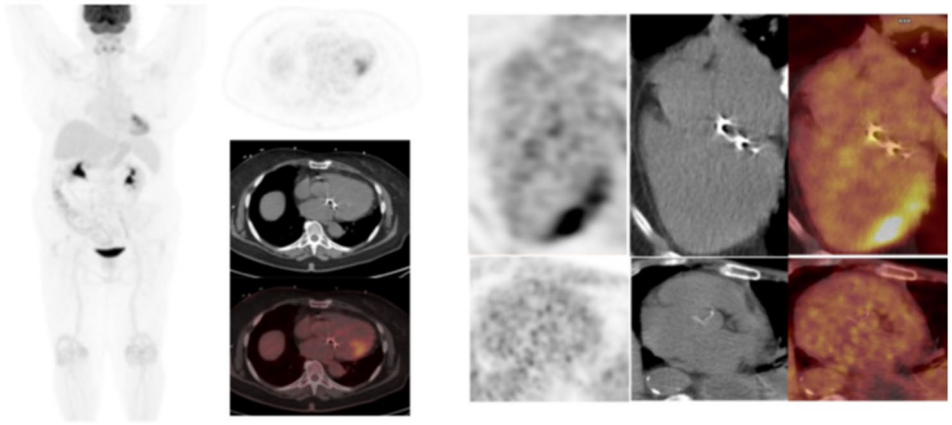

**Fig. 3** [$^{18}$F]FDG PET/CT scan in a patient with mechanical mitral valve endocarditis. The final PET/CT findings rejected the diagnosis of IE as shown by MIP (left panel), transaxial images of the thorax (middle panel bottom-down emission, CT, and superimposed PET/CT) and images reconstructed for valve planes (right panel from left to right emission, CT, and superimposed PET/CT). The uptake seen at the myocardium is due to incomplete suppression of the physiological uptake at the left ventricle wall and papillary muscles which is properly differentiated by accurate image reconstruction. The final diagnosis was a spontaneous rupture of a myocardial cord

truly IE-negative cases, suggesting that radiomics may provide additional discriminatory power even in visually indeterminate cases. However, due to the limited and unbalanced dataset, these findings should be interpreted as exploratory.

### Radiomics-clinical association results

The stratification obtained with the Affinity Propagation clustering resulted in two balanced groups of patients: 173 patients (group 1) and 170 patients (group 2). Group 2 had a higher proportion of PVE with respect to NVE (p-value: 0.004); a higher number of devices (p-value: 0.006); more than 2 major Duke criteria confirmed

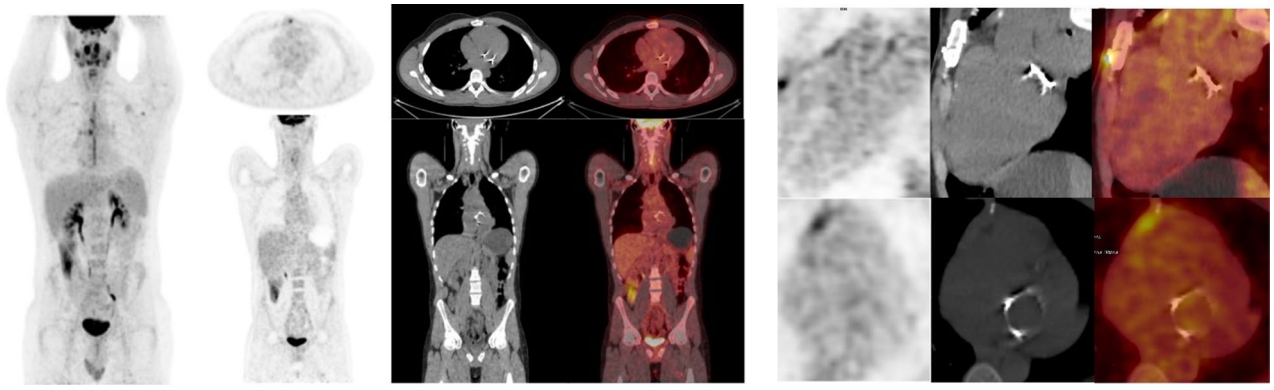

**Fig. 4** [$^{18}$F]FDG PET/CT scan in a patient with biological aortic prosthetic valve endocarditis. Whole body MIP images (left panel), transaxial images of the thorax (middle upper from left to right emission, CT, and superimposed PET/CT) and coronal PET (middle lower from left to right emission, CT, and superimposed PET/CT) and images reconstructed for valve planes (right panel from left to right emission, CT and superimposed PET/CT) ruled out significant uptake in the prosthetic valve, rejecting the diagnosis of IE. The linear uptake on the MIP correspond to physiological uptake of the median arrow

**Table 2** LR models performance

| | Accuracy (mean ± sd) | Sensitivity (mean ± sd) | Specificity (mean ± sd) |
|---|---|---|---|
| **M1** | 0.6605 ± 0.0341 | 0.4123 ± 0.1043 | 0.8123 ± 0.0754 |
| **M2** | 0.6620 ± 0.0396 | 0.4480 ± 0.0844 | 0.7920 ± 0.0693 |
| **M3** | 0.6814 ± 0.0377 | 0.5403 ± 0.0522 | 0.7698 ± 0.0532 |
| **M4** | 0.6991 ± 0.0200 | 0.5743 ± 0.0625 | 0.7769 ± 0.0496 |
| **M5** | 0.6915 ± 0.0470 | 0.5219 ± 0.0972 | 0.7907 ± 0.0755 |
| **M6** | 0.7011 ± 0.0396 | 0.5912 ± 0.0888 | 0.7647 ± 0.0408 |
| **M7** | 0.7315 ± 0.0384 | 0.5995 ± 0.0935 | 0.8154 ± 0.0434 |

Results are provided in terms of mean values ± standard deviation

(p-value < 0.01; a higher proportion of IE positive patients (p-value: 0.002).

### ESC criteria comparison results

The list of regressors included in each model can be found in Supplemental Table 3. Results of LR models are detailed in Table 2. Both Model 1 (M1 – clinical variables only) and Model 2 (M2 – clinical variables and visual [$^{18}$]FDG PET/CT findings) had low sensitivity and similar performance. The addition of radiomics to clinical variables (i.e., M3) improved the model's performance, without significant differences when radiomics was added to visual [$^{18}$]FDG PET/CT analyses (i.e., M4). No differences were also noticed when introducing Duke criteria to the model to the visual assessment of PET/CT (M5). However, performance increased when considering both radiomics and Duke together with clinical variables in M6. The best results were appreciable in M7 which used visual assessment of [$^{18}$]FDG PET/CT, radiomics, Duke criteria and clinical variables (Fig. 5).

## Discussion

To the best of our knowledge, this study represents the largest multicentric investigation focused on the application of radiomics in IE. Our comprehensive analysis and modeling provide a broad overview of the potential

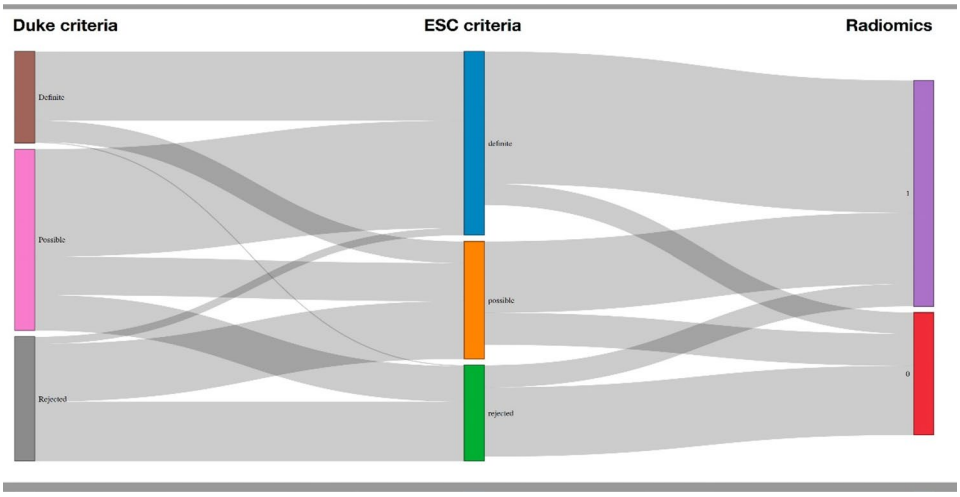


**Fig. 5** Sankey plot for Duke criteria, 2015 ESC criteria and the radiomics-based classification (M7), showing the impact of the final classification of patients

utilization of radiomics in the setting of IE, yielding several notable conclusions. At first, the preliminary descriptive analysis demonstrated the discriminative power of radiomic features, with a significant number of variables emerging as statistically significant in relation to the final diagnosis of IE. In addition, our findings further validated the hypothesis that radiomics can effectively describe and discriminate IE-positive and IE-negative based on visual [$^{18}$F]FDG PET/CT findings. Indeed, we confirmed the diagnostic utility of radiomics in IE, particularly in patients with equivocal [$^{18}$F]FDG PET/CT findings at visual analysis as the random forest model (see Sect. 2.4.2 and 3.4) successfully classified patients as having or not IE. Moreover, the radiomic signature of equivocal PET/CT cases identified by the random forest, closely resembling the signature of IE-negative cases. These results proved that radiomics can be proposed to aid the interpretation of equivocal PET findings at visual analysis, which will be of utmost significance for following the patients' clinical management. Indeed, given the challenges of the diagnosis of cardiovascular infection which requires specialized expertise, radiomics could assist less experienced imagers results in a significant reduction of misleading diagnosis, in particular in equivocal clinical settings. Moreover, radiomics accurately differentiated IE-positive and IE-negative patients even when using an unsupervised approach, which has the benefit of being less sensitive to inherent biases of supervision (see Sect. 2.4.3 and 3.5). Such clustering algorithm successfully associated patients with mild and severe conditions as identified by clinical information, providing a distinct radiomic profiles for the two groups. These profiles can be further assessed and characterized to provide interpretability and explainability within the radiomics framework. It is worth noting that, although the information provided by radiomics was similar to that obtained through visual analysis, it offered unique insights, as shown by the comparison between logistic regression models. Despite the limited increase in accuracy between Model 6 (M6, which included the Duke criteria, clinical data, and the PET radiomic signature) and Model 5 (M5, which the Duke criteria, clinical data and the visual PET assessment), sensitivity improved from 52% to 59%, underscoring the added value of radiomics analysis alongside the visual one. This finding further suggests that texture-based descriptors, imperceptible to the human eye, can provide a more comprehensive assessment of the disease and potentially on one hand expedite the reading of exams and on the other increase consistence of reporting. Notably, the sensitivities of Models 6 and 7— which differed only by the inclusion of one additional regressor in Model 7 (i.e., visual analysis)—were similar; however, specificity was higher for Model 7 (0.8154 ± 0.0434 versus 0.7647 ± 0.0408). The logistic regression results highlighted the crucial impact of variable selection on model performance. overall, the logistic regression models demonstrated that the more comprehensive the information fed into the model, the higher the performance: Model 7, which included the Duke criteria, clinical data, the results of visual [$^{18}$F]FDG PET/CT analyses and radiomics achieved the best accuracy (0.7315 ± 0.0384). However, LR models comparison also suggests the potential for a trade-off between resource demands and performance, which could be further studied and optimized to limit the number of exams needed for an accurate diagnosis. Recently, Gedefroy et al. [26] demonstrated the benefit of using Machine Learning (ML) and radiomics in a cohort of 68 patients with PVE. Interestingly, diagnostic performance of PET-ML in aortic PVE were comparable to our results (59% sensitivity, 83% specificity, 70% balanced accuracy [26] versus 59.95% sensitivity, 81.54% specificity and 73.15% accuracy for M7). Moreover, of utmost importance, our study highlighted the valuable contribution of [$^{18}$F]FDG PET/CT and radiomic signature not only in a larger cohort of PVE patients, but also in NVE, for which literature showed limited role for PET/CT. Specifically, among patients suspected of having NVE, 37 out of 81 (46%) had a positive scan, and the diagnosis was confirmed. In this regard, PET/CT with gating acquisition might further improved diagnostic performance [15].At last, we would like to acknowledge that our study was multicentric, and as such, variability in acquisition parameters, reconstruction protocols, and scanners among centers may have impacted the stability and robustness of radiomic features, consequently affecting the performance of the models [27, 28]. Although reproducibility, harmonization, and the impact of these factors on model performance were beyond the scope of our work, it is important to note that despite the potential pitfalls mentioned above, we obtained promising results comparable to those reported by Gedefroy et al. [26] in a more homogenous cohort. Future assessments could further improve these results through imaging features harmonization strategies via batch-effect removal. Another note to be mentioned for our study is that we provided models' performance based on cross-validation assessments, without explicitly performing external validation. We made this choice due to the inherent heterogeneity of the dataset resulting from its multi-center nature. Cross-validation and bootstrap strategies in fact provide a distribution of performance indices that can be assessed in terms of mean values and standard deviations, unlike single external testing (performed for instance by Gedefroy et al. [26]). In fact, the uncertainty estimation (i.e., standard deviation) plays a crucial role in both ML and statistical models to provide insights into the reliability and robustness of predictions in terms of probabilistic distribution

and to quantify the potential variability and limitations associated with model outputs, informing decision-making and risk management.

Moreover, we analyzed all patients with PVE and NVE together even if they present different uptake patterns. This choice was based on our final goal which was to evaluate the applicability of radiomic model in endocarditis, beyond the traditional uptake pattern. Lastly, we acknowledged that the ESC 2023 criteria [3] are the current recommended. However, since this multicenter cohort dates back to 2015–2020 and patients were managed according to the ESC 2015 criteria, we used this referral classification to avoid bias.

## Conclusions

Radiomic signature effectively described and discriminated [$^{18}$F]FDG PET/CT outcome in a large cohort of patients with IE, identifying a specific signature of equivocal PET/CT findings. Our results suggested that radiomics features can aid the interpretation of equivocal PET findings at visual analysis, significantly impacting on clinical management. Moreover, our clustering algorithm successfully associated patients with mild and severe conditions which can be further assessed and characterized to provide interpretability and explainability within the radiomic framework in a risk score fashion.

**Abbreviations**

| | |
|---|---|
| AC | Attenuation-corrected |
| CI | Confidence interva |
| CT | Computed tomography |
| DICOM | Digital imaging and communications in medicine |
| EANM | European association of nuclear medicine |
| ESC | European society of cardiology |
| EURO-ENDO | European infective endocarditis registry |
| [$^{18}$F]FDG | Fluorine-18 fluorodeoxyglucose |
| FWHM | Full width at half maximum |
| GLCM | Gray level co-occurrence matrix |
| HFLC | High-fat and low-carbohydrate |
| IBSI | Imaging biomarkers standardization initiative |
| ICD | Implantable cardioverter defibrillator |
| IE | Infective endocarditis |
| MIP | Maximum intensity projection |
| MSSA | Methicillin-sensitive staphylococcus aureus |
| NAC | Nonattenuation corrected |
| NVE | Native valve endocarditis |
| OOB | Out-of-bag |
| PCA | Principal component analysis |
| PET/CT | Positron emission tomography/computed tomography |
| PET VCAR | Positron emission tomography volume computer assisted reading |
| PM | Pace maker |
| PVE | Prosthetic valve endocarditis |
| ROI | Region of interest |
| SMOTE | Synthetic minority over-sampling technique |
| SUV | Standard uptake value |
| TOF | Time of flight |
| VOI | Volume of interest |

## Supplementary Information

The online version contains supplementary material available at https://doi.org/10.1186/s13550-025-01366-9.

Supplementary Material 1

**Acknowledgements**

The authors would like to acknowledge the invaluable contributions of the technical staff, nurses, and referring clinicians in every clinical site, whose expertise and dedication were essential to the enrollment and scanning of the patients participating in this study.

**Author contributions**

The manuscript has been seen and approved by all authors, whose individual contributions were as follows: PAE, RS, MNP and AR contributed to patient enrollment and management; RZ, MS, DTH and SAB supervised data collection and assured accuracy, PAE, AG, MP performed and interpreted PET/CT, RZ, MS, LC, AR, FI performed texture features analysis and radiomics' data modelling, PAE, MS, RS, LC and FI conceptualized the work and wrote the paper.

**Funding**

Nothing to declarefor this specific publication.

**Data availability**

The datasets used and/or analyzed during the current study are available from the corresponding author on reasonable request.

## Declarations

**Ethics approval and consent to participate**

This study was conducted in accordance with the principles of the Declaration of Helsinki. Ethical approval was obtained from the appropriate institutional review board. Informed consent was obtained from all individual participants included in the study. The study has been approved by by Comitato Etico di Area Vasta Nord Ovest (CEAVNO), Sezione Autonoma del Comitato Etico Regionale per la Sperimentazione Clinica, 20511 OR-IMPECt.

**Consent for publication**

Not applicable.

**Competing interests**

All authors declare no competing financial interests for this specific publication.

**Author details**

[1]Department of Medicine and Surgery, University of Milano-Bicocca, Milan, Italy
[2]Nuclear Medicine, Department ASST Papa Giovanni XXIII, Bergamo, Italy
[3]Medical Imaging Center, Department of Nuclear Medicine and Molecular Imaging, University of Groningen, University Medical Center Groningen, Groningen, The Netherlands
[4]Formerly at Nuclear Medicine, Department of Translational Research and Advanced Technology in Medicine, University of Pisa and Pisa University Hospital, Via Roma 67, Pisa 56123, Italy
[5]Department of Biomedical Sciences, Humanitas University, Via Rita Levi Montalcini 4, Pieve Emanuele (Milan), Italy
[6]IRCCS Humanitas Research Hospital, Rozzano (Milan), Italy
[7]Faculty of Medicine and Surgery, Vita-Salute San Raffaele University, Milano, Italy
[8]Department of Nuclear Medicine, IRCCS Ospedale San Raffaele, Milano, Italy
[9]Department of Mathematics, MOX, Politecnico di Milano, Piazza Leonardo da Vinci 32, Milano 20133, Italy
[10]Universitat Autònoma de Barcelona, Barcelona, Spain
[11]Department of Nuclear Medicine, Hospital Universirtari Vall d'Hebron, Barcelona, Spain
[12]Department of Cardiology, Hospital Universitari Vall d'Hebron, Barcelona, Spain
[13]Department of Radiology, Hospital Universitari Vall d'Hebron, Barcelona, Spain
[14]CHDS – Center for Health Data Science, Human Technopole, Milan, Italy
[15]Department of Biomedical Photonic Imaging, Faculty of Science and Technology, University of Twente, Enschede, the Netherlands

[16]Department of Medicine and Surgery, University of Milano Bicocca and ASST Papa Giovanni XXII, Piazza OMS 1, Bergamo 24127, Italy

Received: 16 July 2025 / Accepted: 22 December 2025
Published online: 14 February 2026

## References


1. Habib G, Erba PA, Iung B, Donal E, Cosyns B, Laroche C, Popescu BA, Prendergast B, Tornos P, Sadeghpour A, et al. Clinical presentation, aetiology and outcome of infective endocarditis. Results of the ESC-EORP EURO-ENDO (European infective endocarditis) registry: a prospective cohort study. Eur Heart J. 2019;40:3222–32.
2. Durack DT, Lukes AS, Bright DK. Duke endocarditis service new criteria for diagnosis of infective endocarditis: utilization of specific echocardiographic findings. Duke endocarditis service. Am J Med. 1994;96:200–9.
3. Delgado V, Ajmone Marsan N, de Waha S, Bonaros N, Brida M, Burri H, Caselli S, Doenst T, Ederhy S, Erba PA et al. 2023 ESC Guidelines for the management of endocarditis: Developed by the task force on the management of endocarditis of the European Society of Cardiology (ESC) Endorsed by the European Association for Cardio-Thoracic Surgery (EACTS) and the European Association of Nuclear Medicine (EANM). *Eur. Heart J.* 2023, *2*.
4. Li JS, Sexton DJ, Mick N, Nettles R, Fowler VG, Ryan T, Bashore T, Corey GR. Proposed modifications to the Duke criteria for the diagnosis of infective endocarditis. Clin Infect Dis. 2000;30:633–8.
5. Habib G, Lancellotti P, Antunes MJ, Bongiorni MG, Casalta J-P, Del Zotti F, Dulgheru R, El Khoury G, Erba PA, Iung B, et al. 2015 ESC guidelines for the management of infective endocarditis. Eur Heart J. 2015;36:ehv319.
6. Saby L, Laas O, Habib G, Cammilleri S, Mancini J, Tessonnier L, Casalta J-P, Gouriet F, Riberi A, Avierinos J-F, et al. Positron emission tomography/computed tomography for diagnosis of prosthetic valve endocarditis: increased valvular 18F-fluorodeoxyglucose uptake as a novel major criterion. J Am Coll Cardiol. 2013;61:2374–82.
7. Rouzet F, Chequer R, Benali K, Lepage L, Ghodbane W, Duval X, et al. Respective performance of 18F-FDG PET and radiolabeled leukocyte scintigraphy for the diagnosis of prosthetic valve endocarditis. J Nucl Med. 2014;55:1980–5.
8. Fagman E, van Essen M, Fredén Lindqvist J, Snygg-Martin U, Bech-Hanssen O, Svensson G. 18F-FDG PET/CT in the diagnosis of prosthetic valve endocarditis. Int J Cardiovasc Imaging. 2016;32:679–86.
9. Ricciardi A, Sordillo P, Ceccarelli L, Maffongelli G, Calisti G, Di Pietro B, et al. 18-fluoro-2-deoxyglucose positron emission tomography-computed tomography: an additional tool in the diagnosis of prosthetic valve endocarditis. Int J Infect Dis. 2014;28:219–24.
10. Bartoletti M, Tumietto F, Fasulo G, Giannella M, Cristini F, Bonfiglioli R, et al. Combined computed tomography and fluorodeoxyglucose positron emission tomography in the diagnosis of prosthetic valve endocarditis: a case series. BMC Res Notes. 2014;7:2–7.
11. Pizzi MN, Roque A, Fernández-Hidalgo N, Cuéllar-Calabria H, Ferreira-González I, Gonzàlez-Alujas MT, Oristrell G, Gracia-Sánchez L, González JJ, Rodríguez-Palomares J, et al. Improving the diagnosis of infective endocarditis in prosthetic valves and intracardiac devices with 18F-Fluordeoxyglucose positron emission tomography/Computed tomography angiography: initial results at an infective endocarditis referral center. Circulation. 2015;132:1113–26.
12. Roque A, Pizzi MN, Cuéllar-Calàbria H, Aguadé-Bruix S. F–FDG-PET/CT angiography for the diagnosis of infective endocarditis. Curr Cardiol Rep. 2017;19:18.
13. Duval X, Le Moing V, Tubiana S, Esposito-Farèse M, Ilic-Habensus E, Leclercq F, Bourdon A, Goehringer F, Selton-Suty C, Chevalier E, et al. Impact of systematic Whole-body 18F-Fluorodeoxyglucose PET/CT on the management of patients suspected of infective endocarditis: the prospective multicenter TEPvENDO study. Clin Infect Dis. 2021;73:393–403.
14. Primus CP, Clay TA, McCue MS, Wong K, Uppal R, Ambekar S, Das S, Bhattacharyya S, Davies LC, Woldman S, et al. 18F-FDG PET/CT improves diagnostic certainty in native and prosthetic valve infective endocarditis over the modified Duke criteria. J Nucl Cardiol. 2022;29:2119–28.
15. Boursier C, Duval X, Bourdon A, Imbert L, Mahida B, Chevalier E, Claudin M, Hoen B, Goehringer F, Selton-Suty C, et al. ECG-Gated cardiac FDG PET acquisitions significantly improve detectability of infective endocarditis. JACC Cardiovasc Imaging. 2020;13:2691–3.
16. Slart RHJA, Glaudemans AWJM, Gheysens O, Lubberink M, Kero T, Dweck MR, et al. Procedural recommendations of cardiac PET/CT imaging: standardization in inflammatory-, infective-, infiltrative-, and innervation (4Is)-related cardiovascular diseases: a joint collaboration of the EACVI and the EANM. Eur J Nucl Med Mol Imaging. 2020. https://doi.org/10.1007/s00259-020-05066-5.
17. Antunovic L, Artesani A, Coniglio M, Oyen WJG, Ciccarelli M, Selmi C, et al. [18F]FDG PET/CT in large vessel vasculitis: the impact of expertise and confounders on image analysis. Diagnostics. 2022. https://doi.org/10.3390/diagnostics12112717.
18. Sollini M, Antunovic L, Chiti A, Kirienko M. Towards clinical application of image mining: a systematic review on artificial intelligence and radiomics. Eur J Nucl Med Mol Imaging. 2019;46:2656–72.
19. Slart RHJA, Williams MC, Juarez-Orozco LE, Rischpler C, Dweck MR, Glaudemans AWJM, Gimelli A, Georgoulias P, Gheysens O, Gaemperli O, et al. Position paper of the EACVI and EANM on artificial intelligence applications in multimodality cardiovascular imaging using SPECT/CT, PET/CT, and cardiac CT. Eur J Nucl Med Mol Imaging. 2021;48:1399–413.
20. Sollini M, Bartoli F, Marciano A, Zanca R, Slart RHJA, Erba PA. Artificial intelligence and hybrid imaging: the best match for personalized medicine in oncology. Eur J Hybrid Imaging. 2020;4:24.
21. Hatt M, Krizsan AK, Rahmim A, Bradshaw TJ, Costa PF, Forgacs A, et al. Joint EANM/SNMMI guideline on radiomics in nuclear medicine : jointly supported by the EANM Physics Committee and the SNMMI Physics, Instrumentation and Data Sciences Council. Eur J Nucl Med Mol Imaging. 2022. https://doi.org/10.1007/s00259-022-06001-6.
22. Roque A, Pizzi MN, Fernández-Hidalgo N, Permanyer E, Cuellar-Calabria H, Romero-Farina G, et al. Morpho-metabolic post-surgical patterns of non-infected prosthetic heart valves by [18F]FDG PET/CTA: "normality" is a possible diagnosis. Eur Heart J. 2020;21:24–33.
23. Nioche C, Orlhac F, Boughdad S, Reuze S, Goya-Outi J, Robert C, et al. Lifex: a freeware for radiomic feature calculation in multimodality imaging to accelerate advances in the characterization of tumor heterogeneity. Cancer Res. 2018;78:4786–9.
24. Zwanenburg A, Leger S, Vallières M, Löck S. Initiative, for the I.B.S. Image Biomark standardisation initiative. 2016.
25. Frey BJ, Dueck D. Clustering by passing messages between data points. Science. 2007;315:972–6.
26. Godefroy T, Frécon G, Asquier-Khati A, Mateus D, Lecomte R, Rizkallah M, et al. 18F-FDG-based radiomics and machine learning: useful help for aortic prosthetic valve infective endocarditis diagnosis? JACC Cardiovasc Imaging. 2023;16:951–61.
27. Cavinato L, Gozzi N, Sollini M, Kirienko M, Carlo-Stella C, Rusconi C, et al. Explainable domain transfer of distant supervised cancer subtyping model via imaging-based rules extraction. Artif Intell Med. 2023. https://doi.org/10.1016/j.artmed.2023.102522.
28. Orlhac F, Boughdad S, Philippe C, Stalla-Bourdillon H, Nioche C, Champion L, Soussan M, Frouin F, Frouin V, Buvat I. A postreconstruction harmonization method for multicenter radiomic studies in PET. J Nucl Med. 2018;59:1321–8.


## Publisher's note